In situ pyrolysis of ZIF-67 with cobalt nitrate etching for the catalytic oxidation of methane: Promoting surface lattice oxygen and molecular oxygen activation

Yuyang Liu,[a] Xiaofeng Wang,[a,*] Birong Miao,[a] Qianji Chu,[a] Yanghui Mao,[a] Rui Zhang,[b] Qingbo Li[a]

[a] Green Shipping and Carbon Neutrality Lab, College of Environmental Science and Engineering, Dalian Maritime University, Dalian 116026, China

[b] China Academy of Transportation Sciences, Beijing 100029, China

* Corresponding author, email: Xiaofeng Wang, wangxf@dlmu.edu.cn

This file includes:

1. Catalyst Characterizations

1.1. X-ray powder diffraction (XRD)

XRD was performed on a Panalytical X'Pert Pro diffractometer using Cu-Kα radiation source. The data were collected from 10 to 90° with a scanning speed of 5°/min at room temperature. Crystal size was calculated as Scherrer equation: $D = \frac{0.89\lambda}{\beta cos\theta}$, where λ, β and θ denoted the X-ray wavelength (nm), full wave at half maximum and diffraction angle, respectively.

1.2. Raman

Raman spectra was measured on a Horiba LabRAM HR Evolution Raman Spectrometer under ambient condition using a laser with a wavelength of 532 nm. The spectra were recorded using a scan number from 100 to 800 cm^{-1}.

1.3. N_2 adsorption-desorption measurements

Before analysis, the samples were degassed at 300 °C for 8 h. Nitrogen adsorption and desorption isotherms of substrates and catalysts were obtained at -196 ºC. The surface area and the total pore volume of the samples were calculated using the Brunauer-Emmett-Teller (BET) method in a relative pressure range of 0.05-0.25 and the adsorption quantity at a relative pressure of $P/P_0 = 1.0$, respectively.

1.4. X-ray photoelectron spectroscopy (XPS)

XPS was conducted on a Thermo Scientific K-Alpha spectrometer using a

monochromatic Al Kα radiation (hν= 1486.6 eV), at a take-off angle of 0°. The survey scan spectra, Co 2p, and O 1s core level spectra were recorded at a pass energy of 30 eV. Correction of the charge effect was made with the C1s peak at 284.8 eV.

1.5. Electron paramagnetic resonance (EPR)

EPR spectra was obtained on an electron paramagnetic resonance spectrometer (Bruker, E500) at room temperature.

1.6. Temperature-programmed experiments

Temperature-programmed experiments was carried out on the BJBUILDER PCA1200 Chemisorbent Analyzer equipment using the thermal conductivity detector (TCD) as a detector.

For H_2-TPR, 0.05 g sample was firstly pretreated at 300 °C for 1 h with a pure Ar flow (30 mL/min), and then cooled to 50 °C. 10 vol% H_2/Ar with a flow rate of 30 mL/min as the reducing gas was introduced and the reactor was heated from 50 °C to 700 °C with a rate of 10 °C/min.

For O_2-TPD, 0.1g sample was pretreated by pure Ar (30 mL/min) at 400 °C for 30 min and then the sample was treated with pure O_2 for 30 min and cool down to 50 °C in pure Ar. After that, sample was heated from 50 to 950 °C with a rate of 10 °C/min.

For Ar-TPD, 0.1g sample was pretreated by pure Ar or 2 vol% CH_4 (30 mL/min) at 300 °C for 30 min and then the sample was cooling down to 50 °C in pure Ar. After

that, sample was heated from 50 to 950 °C with a rate of 10 °C/min.

For CH_4-TPR, 0.1g sample was pretreated at 200 °C for 1 h with a pure Ar flow (30 mL/min), and then cooled to 50 °C. 10 vol% CH_4/Ar with a flow rate of 30 mL/min as the reducing gas was introduced and the reactor was heated from 50 °C to 550 °C with a rate of 10 °C/min.

1.7. In-situ diffuse reflectance infrared Fourier transform spectroscopy (in situ DRIFTS)

In-situ DRIFTS measurements were collected with a Nicolet Nexus spectrometer equipped with a liquid nitrogen-cooled MCT detector. The catalyst was pretreated in N_2 (50 mL/min) at 200 °C for 30 min and then cooled to 50 °C. Next, the flow gas was switched to 1 vol% CH_4 and 99 vol% N_2 and the spectra were recorded from 50 to 400 °C. Then 20 vol% O_2 was introduced into the system and the spectra were recorded from 1 to 25 min at 400 °C.

2. Figures and Tables

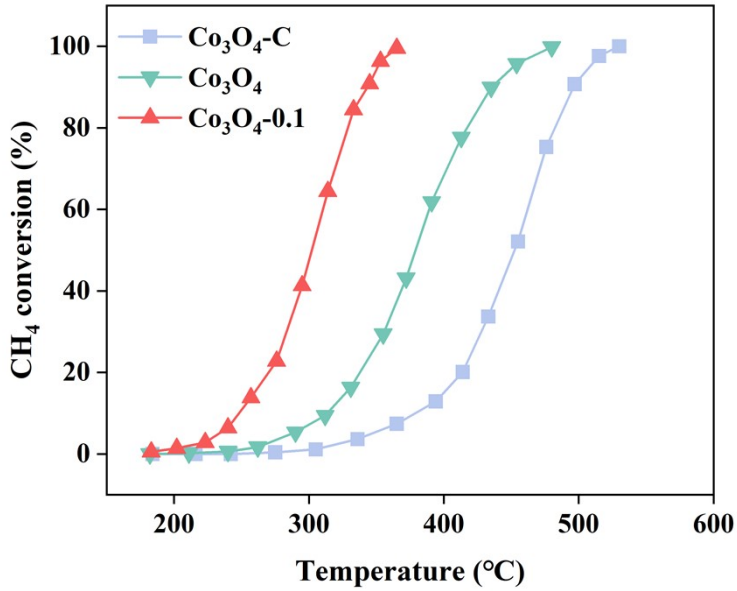

Figure S1. CH_4 conversion (reaction condition: 1 vol% CH_4, 20 vol% O_2 and 79 vol% N_2, WHSV= 30,000 $mL \cdot g^{-1} \cdot h^{-1}$) of Co_3O_4, Co_3O_4-0.1 and Co_3O_4-C catalysts.

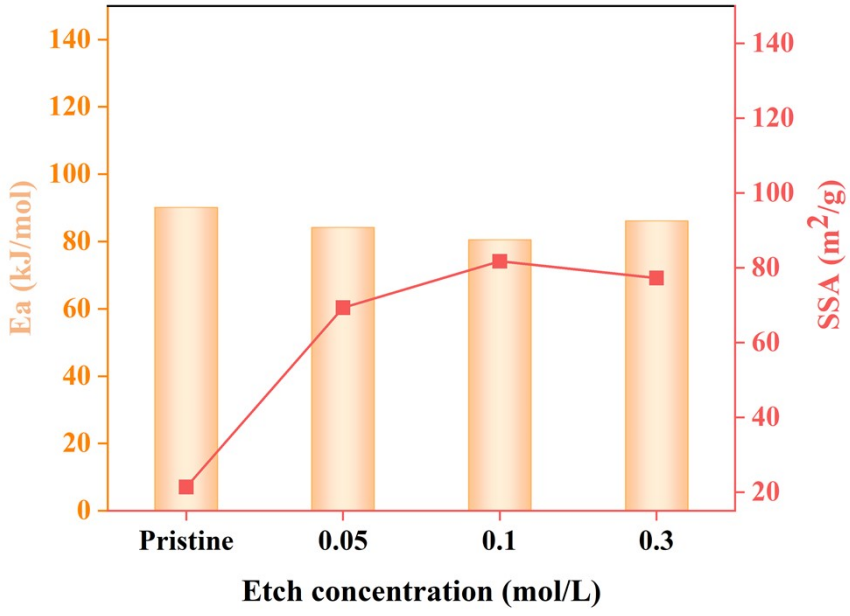

Figure S2. Relationship between etching conditions and catalyst activity as well as specific surface area.

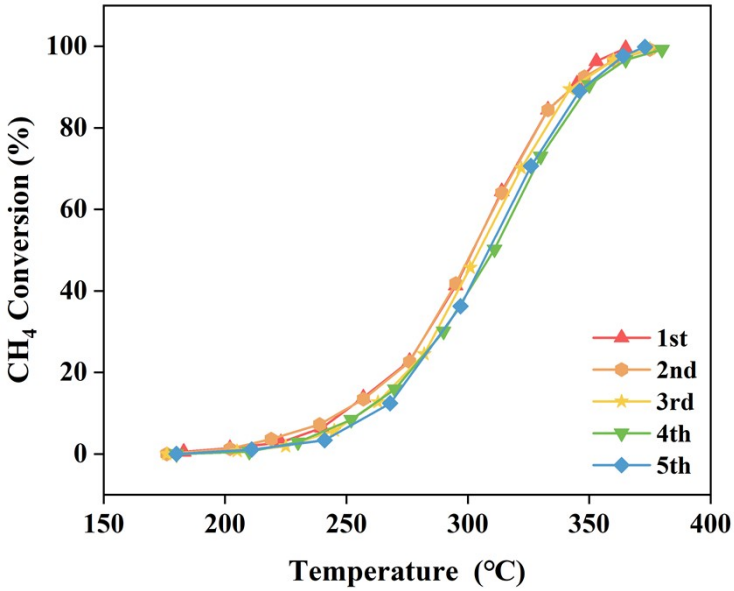

Figure S3. Cycling test results of Co_3O_4-0.1 catalyst for 5 times (reaction condition: 1 vol% CH_4, 20 vol% O_2 and N_2 as a balance gas, WHSV= 30,000 $mL \cdot g^{-1} \cdot h^{-1}$).

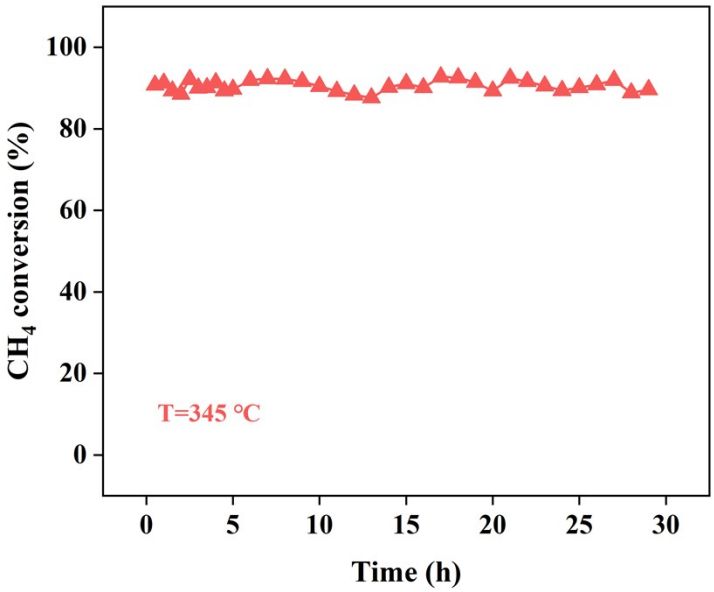

Figure S4. Long-term testing of Co_3O_4-0.1 catalyst (reaction condition: 1 vol% CH_4, 20 vol% O_2 and 79 vol% N_2, WHSV= 30,000 $mL \cdot g^{-1} \cdot h^{-1}$) of Co_3O_4, Co_3O_4-0.1 and Co_3O_4-C catalysts.

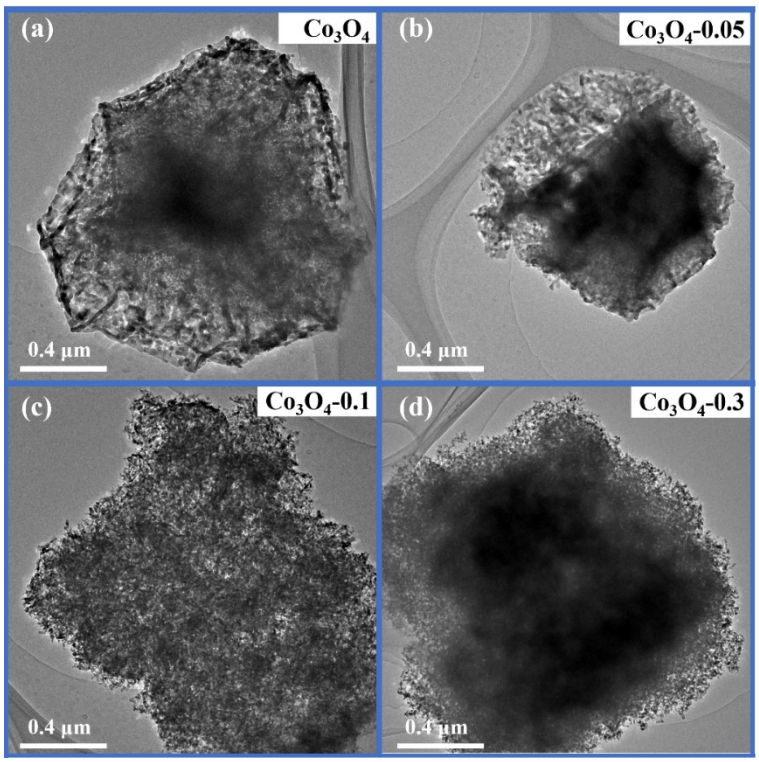

Figure S5. TEM images of (a) Co_3O_4, (b) Co_3O_4-0.05, (c) Co_3O_4-0.1 and (d) Co_3O_4-0.3 catalysts.

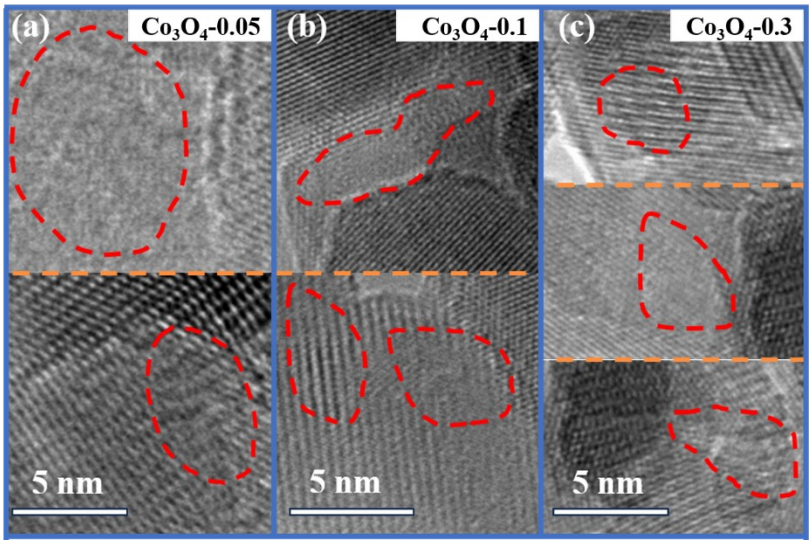

Figure S6. Lattice defect regions (marked with red dotted lines) of (a) Co_3O_4-0.05, (b) Co_3O_4-0.1 and (c) Co_3O_4-0.3 catalyst.

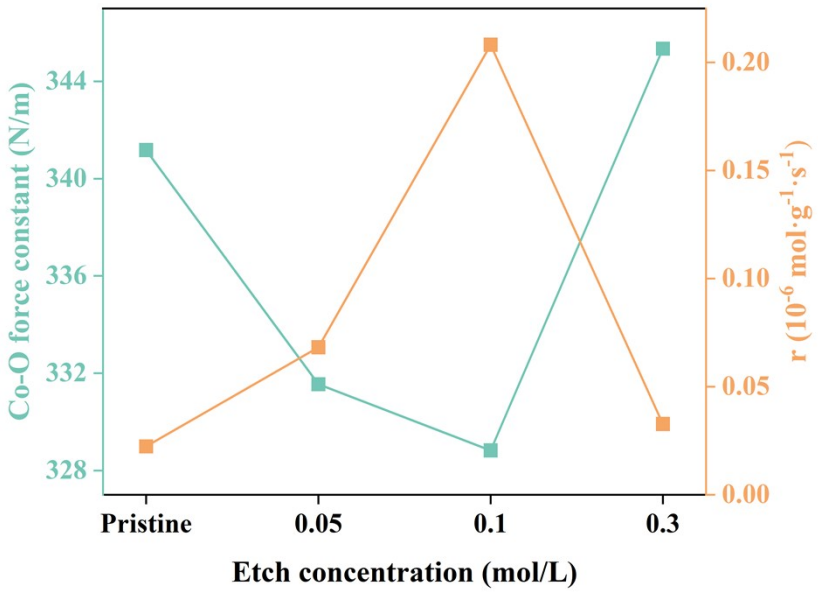

Figure S7. Relationship between etching conditions and catalyst activity as well as strength of Co-O bonds.

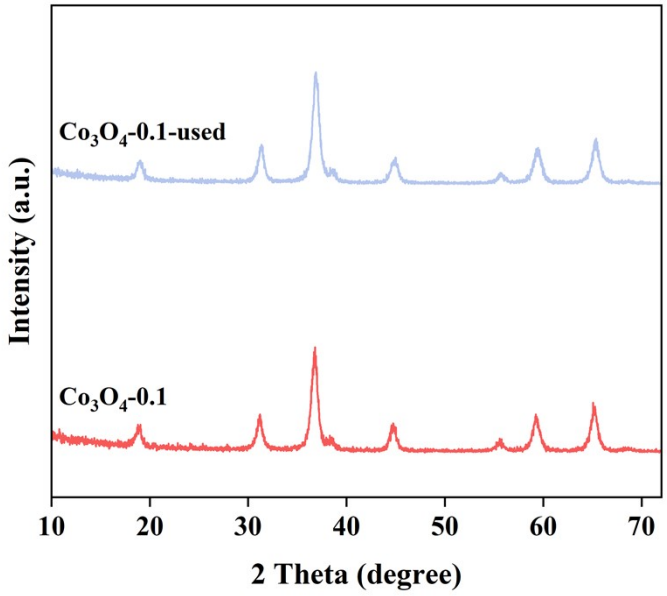

Figure S8. XRD spectra of Co_3O_4-0.1 catalyst before and after the long-term test.

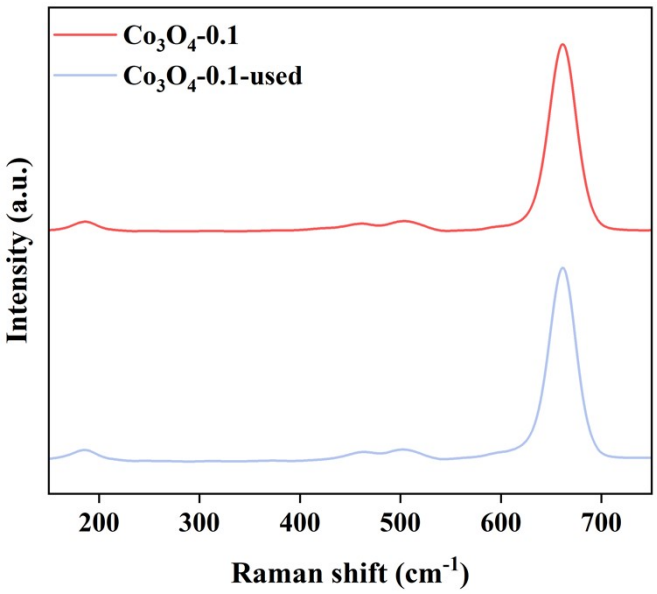

Figure S9. Raman spectra of Co_3O_4-0.1 catalyst before and after the long-term test.

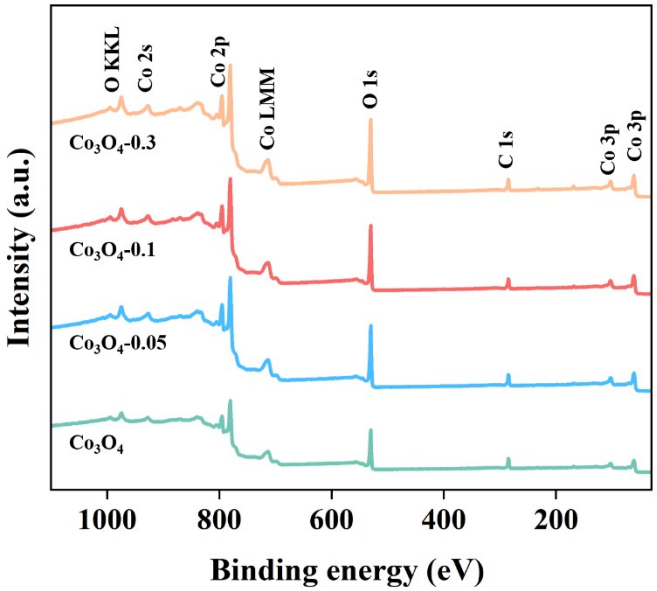

Figure S10. XPS full spectra of all catalysts.

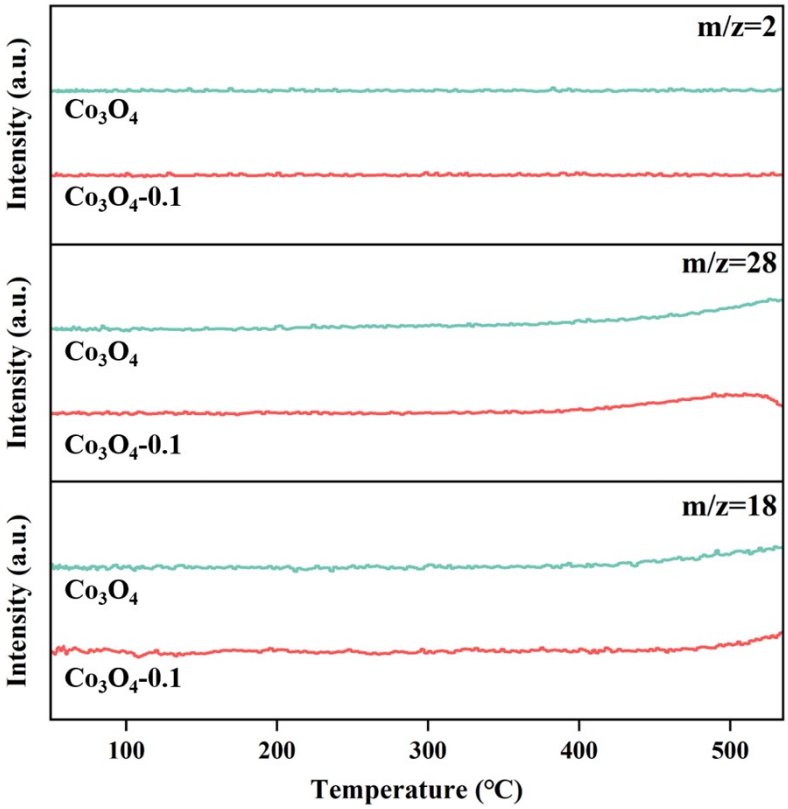

Figure S11. H_2, CO and H_2O signals from CH_4-TPR of Co_3O_4 and Co_3O_4-0.1 catalysts.

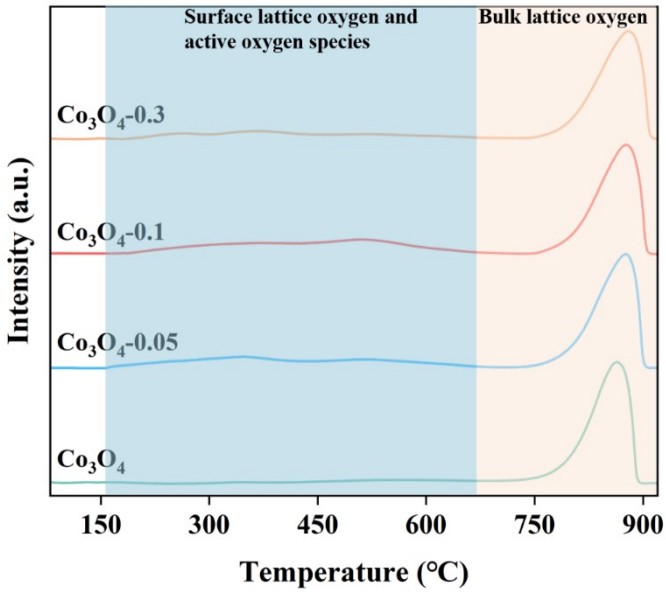

Figure S12. O_2-TPD profiles of all catalysts.

Table S1. Performance comparison with other catalysts for CH_4 oxidation.

Catalysts	T_{90}(°C)	Reaction condition	Ref.
Co_3O_4-r	385	1 vol% CH_4 and 99 vol% air, SV = 30,000 mL g^{-1} h^{-1}	[1]
Co_3O_4-9.0	413	0.5 vol% CH_4, 8 O_2 vol% and balanced with N_2, SV = 18,000 mL g^{-1} h^{-1}	[2]
$La_{0.85}Ce_{0.15}CoO_3$	486	0.5 vol% CH_4, 8 O_2 vol% and balanced with N_2, SV = 30,000 mL g^{-1} h^{-1}	[3]
Co_3O_4/H-ZSM-5	409	1 vol% CH_4 and 99 vol% air, SV = 20,000 mL g^{-1} h^{-1}	[4]
$Co_3O_4/La_2O_2CO_3/LaCoO_3$	476	1 vol% CH_4 and 99 vol% air, SV = 15,000 mL g^{-1} h^{-1}	[5]
5 wt% La-Co_3O_4	661	2 vol% CH_4 and 98 vol% air, SV = 6,000 mL g^{-1} h^{-1}	[6]
1 wt% Pd/Co_3O_4	361	1 vol% CH_4,20 O_2 vol% and balanced with N_2, SV = 30,000 mL g^{-1} h^{-1}	[7]
Co_3O_4-0.1	**345**	**1 vol% CH_4, 20 vol% O_2 in N_2, SV = 30,000 mL g^{-1} h^{-1}**	**This work**

Table S2. Physical and chemical properties of prepared Co_3O_4 catalysts.

Sample	Crystal size [a] (nm)	Surface area [b] (m^2 g^{-1})	Pore diameter [c] (nm)	Co^{3+}/Co^{2+} [d] (%)	O_{ads}/O_{latt} [d] (%)
Co_3O_4	23.8	21.3	9.5	2.04	0.34
Co_3O_4-0.05	11.1	69.3	2.2	2.5	0.39
Co_3O_4-0.1	11.2	81.7	33.0	2.63	0.42
Co_3O4-0.3	11.0	86.1	33.2	2.17	0.5

[a] Crystal size obtained from the results of XRD;

[b] Calculated by BET method;

[c] Calculated by BJH method;

[d] Calculated based on XPS results.

References

[1] Yihang Jiang, Wenzhi Li, Kun Chen, Xia Zhang, Changcheng Shen, and Liang Yuan, A rod-like Co_3O_4 with high efficiency and large specific surface area for lean methane catalytic oxidation. *Molecular Catalysis*, 2022. **522**: p. 112229.

[2] Yifan Zheng, Yan Liu, Huan Zhou, Wanzhen Huang, and Zhiying Pu, Complete combustion of methane over Co_3O_4 catalysts: Influence of pH values. *Journal of Alloys and Compounds*, 2018. **734**: p. 112-120.

[3] Lei Jiang, Danyang Li, Guixian Deng, Chunqiang Lu, Linan Huang, Zhiqiang Li, Haiwen Xu, Xing Zhu, Hua Wang, and Kongzhai Li, Design of hybrid $La_{1-x}Ce_xCoO_{3-\delta}$ catalysts for lean methane combustion via creating active Co and Ce species. *Chemical Engineering Journal*, 2023. **456**: p. 141054.

[4] Chao Fan, Zhiwei Wu, Zhikai Li, Zhangfeng Qin, Huaqing Zhu, Mei Dong, Jianguo Wang, and Weibin Fan, Controllable preparation of ultrafine Co_3O_4 nanoparticles on H-ZSM-5 with superior catalytic performance in lean methane combustion. *Fuel*, 2023. **334**: p. 126815.

[5] Yahan Wang, Saifei Wang, Jingyu Bai, Long Zhang, Shiguang Zhao, Jiguang Deng, Xiaolong Tang, and Erhong Duan, Structural evolution in $LaCoO_3$ by polyol treatment: Highly active and resistant $Co_3O_4/La_2O_2CO_3/LaCoO_3$

heterostructure catalysts for CH_4 oxidation. *Applied Catalysis B: Environmental*, 2023. **338**: p. 123079.

[6] Yulong Wang, Yating Lv, Yijia Cao, Jinyan Xiao, Pengfei Tu, Lei Yang, Shengwei Tang, and Wenxiang Tang, In-situ reconstruction of $LaCoO_3$-Co_3O_4 hetero-interface over lanthanum modified Co_3O_4 nanocatalyst for improved catalytic activity and sintering resistance in methane combustion. *Catalysis Today*, 2024. **435**: p. 114697.

[7] Juxia Xiong, Kang Wu, Ji Yang, Peng Liu, Linghe Song, Jing Zhang, Mingli Fu, Liming Chen, Haomin Huang, Junliang Wu, and Daiqi Ye, The effect of existence states of PdO_x supported by Co_3O_4 nanoplatelets on catalytic oxidation of methane. *Applied Surface Science*, 2021. **539**: p. 148211.